An Immersed Boundary Method to Simulate Compressible Reactive Flows featuring Shock-Wave Interactions with Three-Dimensional Solid Obstacles

Radouan Boukharfane[1], Benjamin Bouvelle[1], Zakaria Bouali[1], Arnaud Mura[1]
[1]Institut Pprime UPR 3346 CNRS, ISAE ENSMA and University of Poitiers, France

1. Abstract

The present paper describes the development and implementation of an immersed boundary method (IB) aimed at simulating compressible reactive flows around three-dimensional complex solid bodies. The boundaries of the immersed objects are represented with a finite number of Lagrangian points, which are distributed over the fluid-solid interface. The flowfield is described with a fully compressible reactive multicomponent Navier-Stokes solver that makes use of high-order numerical schemes applied to structured Cartesian grids. The corresponding density-based finite difference numerical scheme is thus suited to compressible reactive flows representative of either combustion in high-speed flows or detonation, see Martìnez Ferrer *et al.* [1]. The numerical algorithm is based on a third-order accurate Total Variation Diminishing (TVD) Runge Kutta time integration scheme. It employs a seventh-order accurate Weighted Essentially Non-Oscillatory (WENO) scheme to discretize the non-linear advective terms while an eighth-order accurate centered finite difference scheme is retained for the molecular viscous and diffusive contributions. The numerical solver thus offers an interesting combination of existing methods suited to the present purpose of studying compressible reactive flows featuring shock-wave interaction with three-dimensional solid obstacles. The immersed boundary methodology makes uses of a combined direct forcing approach and ghost-cell technique, which guarantees the imposition of no-slip boundary conditions over the fluid-body interface. The main features of this immersed boundary methodology are described below with special emphasis placed on the treatment of boundary conditions at the immersed surface. The resulting solver has been verified by considering a complete procedure that gathers several elementary verification subsets including, among others, two-dimensional subsonic and supersonic flows around a cylinder, flow over a circular bump, subsonic Blasius flow over a flat plate, etc. The performance of the new algorithm are illustrated herein on three distinct geometries: (i) the two-dimensional supersonic non-reactive flow of air around a cylinder, (ii) the two-dimensional moving-shock/prism interaction and (iii) the three-dimensional flow developing around spherical-nosed projectiles fired into hydrogen-air mixtures at detonative speeds.

2. Immersed boundary set-up procedure

The classical STereo-Lithography (STL) format is employed for representing the three-dimensional triangulated fluid-solid interface. The coordinates of the three vertices of each elementary triangle $T_k, k = 1, \cdots, N$, where N is the number of Lagrangian triangles, allows to define the Lagrangian points as its center of gravity (see Fig.1). Once the Cartesian structured computational grid generated, the geometrical IBM module first performs a flagging step that discriminates between solid and fluid vertices. This numerical procedure relies on a modified ray-tracing algorithm, see Möller and Trumbore [2]. Incorrect surface representations may lead the algorithm to fail, which is secondly corrected thanks to the consideration of additional random rays. Thus, a marker variable field $M(\boldsymbol{x}, t)$ is initialized to identify

Correspondence to: radouan.boukharfane@ensma.fr.fr

the fluid and solid domains:

$$M(\boldsymbol{x},t)=\left\{\zeta_{mnp}, m=1,\cdots,N_{x_1}, n=1,\cdots,N_{x_2}, p=1,\cdots,N_{x_3}\right\}, \tag{1}$$

where N_{x_i} is the number of points in the x_i-direction and

$$\zeta_{mnp}=\begin{cases}1 \text{ if } \boldsymbol{x}=(x_1,x_2,x_3)^t\in\Omega_{fluid},\\ 0 \text{ otherwise}\end{cases} \tag{2}$$

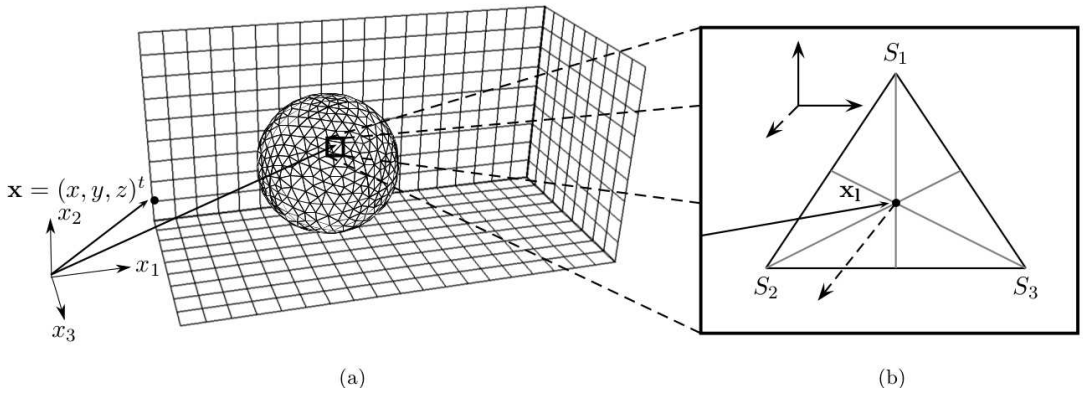

Fig. 1 Immersed boundary in a Cartesian mesh. (a): Cartesian mesh depicted together with the unstructured mesh of the immersed boundary surface, (b): definition of a Lagrangian point $\boldsymbol{x_l}$

Thus, the set of Cartesian grid points belonging to fluid and solid domain are defined by:

$$\Omega_{fluid}=\left\{(x_1,x_2,x_3)^t\in\Omega \text{ with } \zeta_{mnp}=1\right\},\ \Omega_{solid}=\left\{(x_1,x_2,x_3)^t\in\Omega \text{ with } \zeta_{mnp}=0\right\} \tag{3}$$

Note that (i) we have $\Omega_{fluid}\cup\Omega_{solid}=\Omega$, and (ii) $\Omega_{fluid}\cap\Omega_{solid}$ denotes the fluid-solid interface.

The solid points having at-least one fluid neighbour (ghost point GP in Fig.2) are identified as :

$$\Omega_{\text{GP}}=\left\{(x_m,y_n,z_p)^t\in\Omega_{\text{solid}} \text{ if } \exists(x_i,y_j,z_k)^t\in\Omega_{\text{fluid}} \text{ s.t. } i\in I_m\vee j\in I_n\vee k\in I_p\right\} \tag{4}$$

where I_m=$[m-3,m+3]$, I_n=$[n-3,n+3]$ and I_p=$[n-3,n+3]$. From each ghost point, a vector normal to the nearest boundary triangle is built to locate the image of the corresponding ghost point that belongs to the fluid domain. The flowfield variables at each image point are then interpolated from the surrounding computational nodes. The corresponding flowfield variables are subsequently reflected back to the corresponding ghost points to ensure the requisite zero-flux boundary conditions. The definition of Ω_{GP} includes at least three layers of ghost points, which are needed for the seventh-order WENO flux interpolation. Note that this is the same requirement as the one requested for standard ghost points at the boundaries of the computational domain [1]. The unique image point associated with a ghost point is defined as:

$$G_{\text{IP}}=\{(x^*,y^*,z^*)\in\Omega_{\text{fluid}} \text{ s.t. } \exists!(x,y,z)\in G_{\text{GP}}\ \wedge\ D\left[(x^*,y^*,z^*)\perp T\right]=D\left[(x,y,z)\perp T\right]\} \tag{5}$$

where $D\left[(x,y,z)\perp T\right]$ represents the orthogonal distance from a given point (x,y,z) to the elementary triangle T_k, which is the closest to (x,y,z) . The following linear approximation is used to impose a Neumann boundary conditions for solid-fluid interface and fix the flow-field variables at any ghost point, $\varphi_{\text{GP}}=\varphi_{\text{IP}}$ where φ is a given variable. To proceed with this condition, one needs to fix the representative flow-field variables at each image point. This can be achieved by using different interpolation techniques, exploiting the available flowfield variables at the eight surrounding neighbouring nodes NP_k

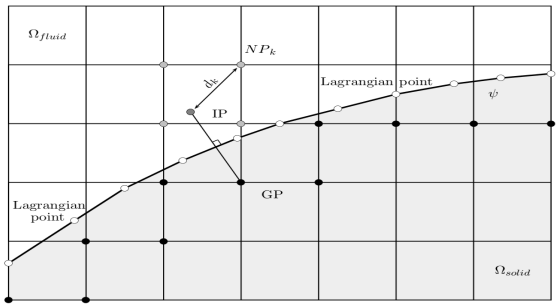

Fig. 2 Immersed boundary procedure. Ω_{solid}, solid domain; Ω_{fluid}, fluid domain; GP, ghost point; BP, boundary point; IP, image point; NP, neighbor points in fluid domain corresponding to each IP.

with $k = 1, \cdots, 8$ (see Fig.2 for the 2D case). Each element of G_{GP} can indeed be associated with four computational nodes:

$$\varphi_{\text{IP}} = \sum_{k=1}^{4} \Phi_k \varphi_{NP_k} \text{ where } \Phi_k = \frac{\eta_k}{d_k^2} \left(\sum_{j=1}^{4} \frac{1}{d_j^2} \right)^{-1} \tag{6}$$

d_k being the distance of the corresponding image point from each NP_k and $\eta_k = 0$ if $NP_k \in \Omega_{\text{fluid}}$ and 1 otherwise. For cases arising from $d_k \to 0$, contribution of NP_l $(l \neq k)$ can be neglected to enforce $\varphi_{\text{IP}} = \varphi_{\text{NP}_k}$. In this work, d_k is considered to be negligible if $d_k/d \leq \epsilon$, with $\epsilon = 10^{-10}$ and $d = \sqrt{\Delta x^2 + \Delta y^2 + \Delta z^2}$, where Δx, Δy, Δz are grid spacing. The flow-field parameters at the image points are then evaluated from

$$T_{\text{IP}} = \sum_{k=1}^{4} \Phi_k T_{NP_k},\ P_{\text{IP}} = \sum_{k=1}^{4} \Phi_k \rho_{NP_k} T_{NP_k} R/\mathcal{W}_{NP_k},\ Y_{\alpha_{\text{IP}}} = \sum_{k=1}^{4} \Phi_k Y_{\alpha_{NP_k}} \tag{7}$$

where $\mathcal{W}$ denotes the molecular mass of the mixture, and R is the universal gas constant. The molecular mass and density at the image points are calculated from

$$\mathcal{W}_{\text{IP}} = \left(\sum_{\alpha=1}^{N} Y_{\alpha_{\text{IP}}}/\mathcal{W}_\alpha \right)^{-1},\ \rho_{\text{IP}} = P_{\text{IP}} \mathcal{W}_{\text{IP}}/R T_{\text{IP}} \tag{8}$$

where $\mathcal{W}_\alpha$ is the molecular mass of the α-species. In this study, the method is used to model an adiabatic boundary and, from a numerical standpoint, adiabatic wall conditions are straightforwardly obtained from:

$$u_n|_{\text{wall}} = 0,\ \left.\frac{\partial u_t}{\partial \boldsymbol{n}}\right|_{\text{wall}} = 0,\ \left.\frac{\partial T}{\partial \boldsymbol{n}}\right|_{\text{wall}} = 0,\ \left.\frac{\partial P}{\partial \boldsymbol{n}}\right|_{\text{wall}} = 0 \tag{9}$$

This is equivalent to state that $u_{n_{\text{IP}}} = 0,\ u_{t_{\text{IP}}} = u_{t_{\text{GP}}},\ T_{\text{IP}} = T_{\text{GP}}$ and $p_{\text{IP}} = p_{\text{GP}}$.

Finally, at each ghost point, the values of the conservative variables are settled from:

$$\rho_{\text{GP}} = \rho_{\text{IP}} \tag{10}$$

$$(\rho u_i)_{\text{GP}} = \rho_{\text{IP}} u_{i_{\text{IP}}},\quad i = 1, \cdots, 3 \tag{11}$$

$$(\rho e_t)_{\text{GP}} = \rho_{\text{IP}} h_{m_{\text{IP}}} - P_{\text{IP}} + \rho_{\text{IP}} (u_{i_{\text{IP}}} u_{i_{\text{IP}}})/2, \tag{12}$$

$$(\rho Y_\alpha)_{\text{GP}} = \rho_{\text{IP}} Y_{\alpha_{\text{IP}}},\quad \alpha = 1, \cdots, N, \tag{13}$$

3. Results and discussion

3.1. Supersonic flow around a circular obstacle

As a preliminary validation step of the proposed methodology, we simulate a supersonic air flow around a circular cylinder. The free stream Mach number value is set to $M = 3.5$. Dirichlet boundary conditions

are set at the inlet of the computational domain while extrapolation rules are used at the outlet. Slip wall boundary conditions are imposed at top and bottom boundaries. The numerical simulations are performed on a structured, non-uniform, single-block grid featuring 2400×600 computational cells, and the immersed boundary is modelled with 160 Lagragian points (see Fig.3 (a)).

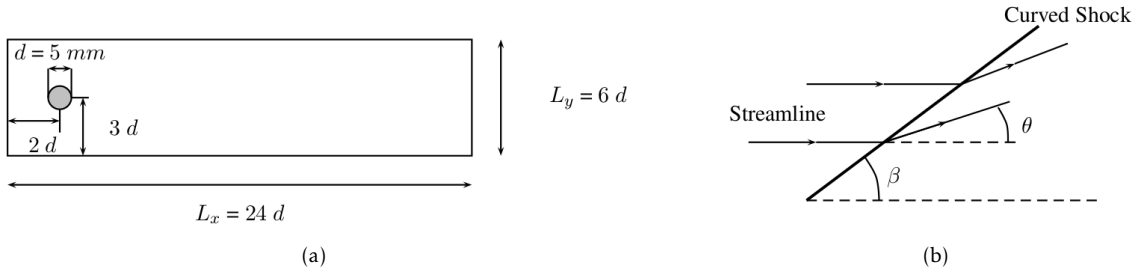

Fig. 3 (a): computational domain with the immersed circular obstacle, (b): schematic view of a deflected supersonic flow and definitions of the angles θ and β.

Fig.4 displays a numerical Schlieren image. From a qualitative point of view, the computed flowfield does not seem to be altered by spurious unphysical pressure oscillations.

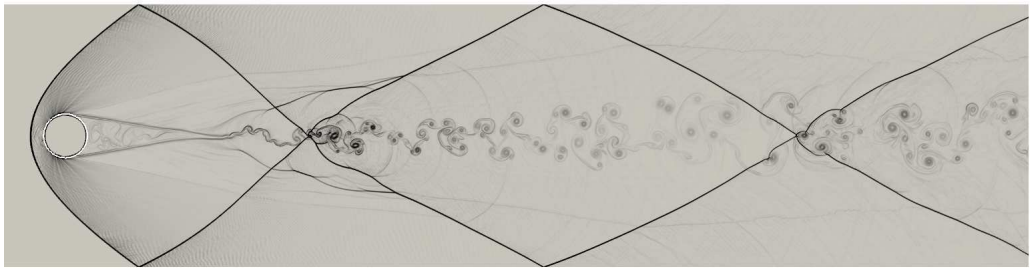

Fig. 4 Supersonic flow over circular cylinder: numerical Schlieren picture

The local properties of the flowfield behind curved detached shocks allow to perform the same type of calculations as the one issued from standard oblique shock-wave relationships:

$$\tan(\theta) = 2\cot(\beta)\left[\frac{M^2\sin^2\beta - 1}{M^2(\gamma + \cos(2\beta)) + 2}\right] \tag{14}$$

where θ is the streamline deflection angle and β is the orientation of the oblique shock-wave relative to the horizontal direction (see Fig.3 (b)).

Fig.5 (a) reports a comparison performed between the expression of (θ, β) given by Eq. 14 and numerical simulation results. The obtained level of agreement is quite satisfactory. Fig.5 (b) displays a comparison performed between the present numerical results and those previously documented by Chaudhuri *et al.* [3]. The quality of the agreement obtained with the computational results issued from the simulation performed on Mesh#3 further confirms the performance of the present methodology.

3.2. Moving-shock/ two-dimensional wedge interaction

The second validation test-case is the impingement of a planar shock on a two dimensional wedge. This problem has been studied experimentally by Schardin [7]. The problem setup is a follows : a Mach 1.30 shock located upstream of the wedge is initialized, when the shock moves across the wedge, the impingement of the planar shock generates a complex compressible flowfield featuring multiple Mach stems and triple points, reflected and scattered shocks, slip lines, acoustic waves and vortices as depicted in Fig.6 . The computational domain is displayed in Fig.7 . Extrapolation rules are used at all

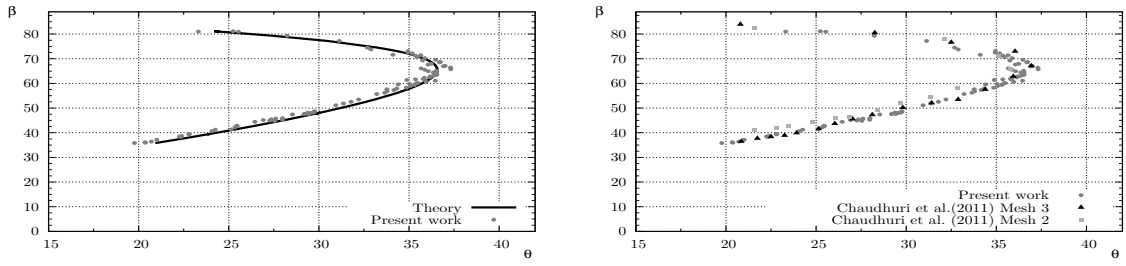

(a) (b)

Fig. 5 Illustration of the (β,θ)-relation ($M = 3.5$), (a): comparison between computational results and Eq. 14, (b): comparison with the results of Chaudhuri *et al.* [3].

boundaries and the computation is performed on a structured grid of $N_x \times N_y = 3501 \times 2501$ cells while the wedge surface is delineated with 1800 Lagrangian points.

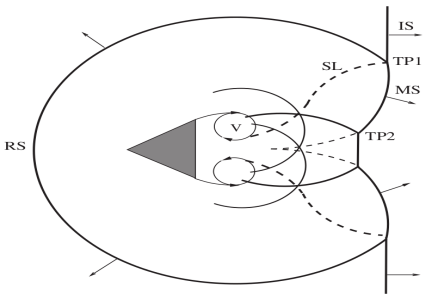

Fig. 6 Various waves arising in Schardin's problem with RS: reflected shock, IS: incident shock, SL: slip line, MS: Mach stem, TP: triple point and V: vortex.

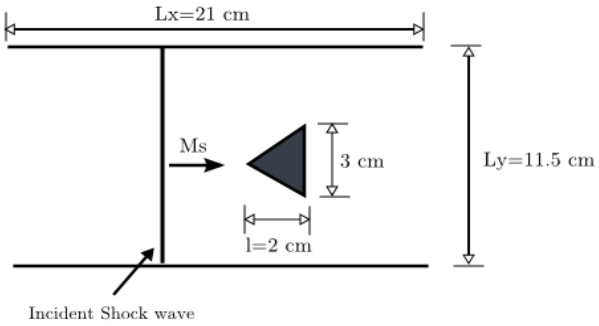

Fig. 7 Sketch of the geometry retained for the computational study of the shock structure passing over a wedge in a channel

Fig.9 highlights the comparison between the present simulation and the results of Chaudhuri *et al.* [3] and Chang and Chang [8] in terms of triple point trajectories and vortex location. It can be seen that the simulated time evolution of the two triple points and the locus of vortex core is in quite good agreement with previous numerical and experimental results. Three instantaneous shadowgraph pictures are compared with the experimental shadowgraph reported in [7]. From Fig.9, It is clear that the numerical method is able to reproduce the global flow characteristics and capture the complex compressible flowfield of Schardin's problem.

□

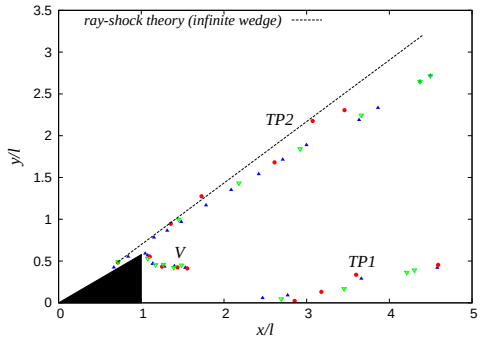

Fig. 8 Triple point trajectories and position of the vortex center (● :experimental data [8], ▽ : numerical results of Chaudhuri *et al.* [3], ▲ : present simulation

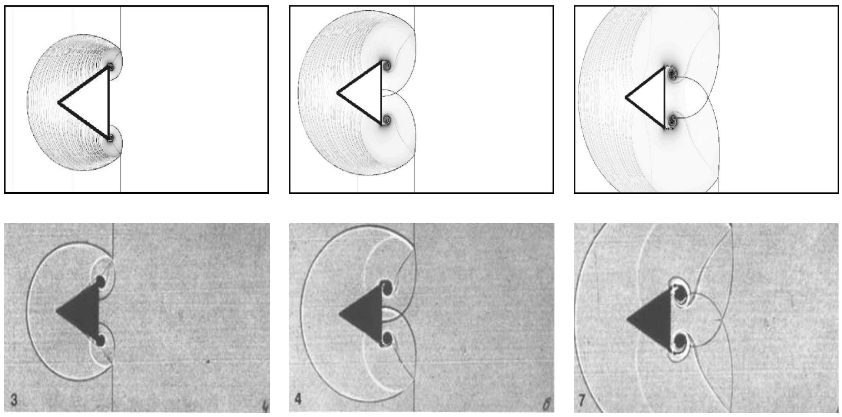

Fig. 9 Snapshots of numerical (top) and experimental (bottom) [7] Schlieren images at different instants

3.3. Hypervelocity spherical-nosed projectile fired into a reactive mixture

Finally, the high-speed projectile experiments of Lehr [5] are considered. The reactive flow is made of a stoichiometric H_2:O_2:N_2 reactive mixture (molar ratios 2:1:3.76). The geometry of the projectile corresponds to a sphere-cylinder of R= 75 mm diameter. The free stream conditions are T_∞ = 293 K and p_∞ = 42.663 kPa and we consider the Mach number condition M = 4.48. These conditions are retained to enable direct comparisons with experimental results gathered by Lehr [5]. Simulations are carried out on a rectangular domain of lengths $L_x \times L_y \times L_z$ = 15R×10R×10R (see Fig.10).

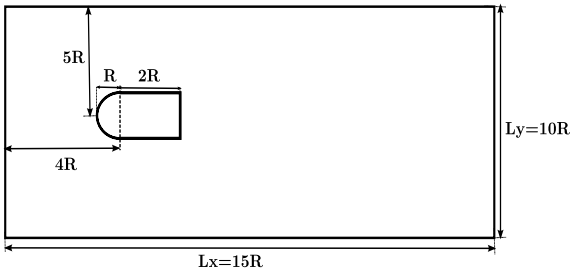

Fig. 10 Sketch of the geometry retained for the computational study of the hypervelocity projectile

The computational mesh is a structured grid featuring approximately 3.6 million cells while the immersed boundary is modelled by using 2600 Lagragian points. The chemical kinetics is described with the detailed mechanism of O'Conaire *et al.* [4] which does involve of 19 elementary reaction steps and 9 chemical species. A preliminary sketch of the obtained computational result is provided in Fig.11 .

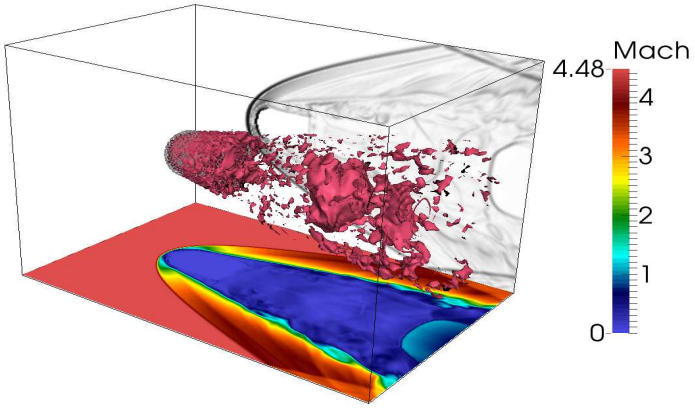

Fig. 11 Supersonic flow around the spherical-nosed projectile. Back: Schlieren snapshot, bottom: Mach number field evaluated in the horizontal median plane from the longitudinal velocity component.

4. Conclusions and prospect

In this paper, we described the implementation of an immersed boundary method (IBM) in a fully compressible reactive multicomponent Navier-Stokes solver that makes use of high-order WENO schemes applied on structured Cartesian grids. The method is successfully applied to the computations of supersonic complex flows of practical interest for high-speed combustion and detonation and thus appears to be well-suited for these conditions. This will allow to simulate flow conditions that are representative of RAM accelerators (RAMAC), which are used to accelerate projectiles to very high velocities [6]. In the present set of numerical simulations, the immersed object was considered to be at rest in high-speed flows; a challenging and natural extension of the present study will therefore concern the application of the same methodology to moving boundaries. It seems that the marker function approach retained herein may provide compelling advantages to deal with such moving bodies.

Acknowledgements. This work is performed in the framework of the Ph.D. Thesis of R. Boukharfane financially supported by Région Poitou-Charentes. The authors are indebted to Prof. Vedovoto (UFU, Brazil) for several discussions and also thank Prof. Chinnayya (ENSMA, Poitiers) for encouraging comments.

References

[1] Martìnez Ferrer P.J., Buttay R., Lehnasch G., Mura A., A detailed verification procedure for reactive multicomponent Navier-Stokes solvers, Computers & Fluids, 89:88–110 (2014).
[2] Möller T., Trumbore B. (1997), Fast, minimum storage ray-triangle intersection, Journal of Graphics Tools, 2:21–28.
[3] Chaudhuri A., Hadjadj A., Chinnayya A. (2011), On the use of immersed boundary methods for shock/obstacle interactions, Journal of Computational Physics, 230:1731–1748.
[4] O'Conaire M., Curran H.J., Simmie J.M., Pitz R.W., Westbrook C.G.(2004), A comprehensive modeling study of hydrogen oxidation, International Journal of Chemical Kinetics, 11:602–622.
[5] Lehr H.F. (1972), Experiments on shock-induced combustion, Astronautica Acta, 17:589–597.
[6] Hertzberg A., Burnham E.A., Hinkey J.B. (1994), Recent advances in RAM accelerator technology, in: *Combustion in high-speed flows*, J. Buckmaster, T.L. Jackson and A. Kumar (Eds.), Kluwer Academic Publishers, pp. 309-344.
[7] Sivier, S., Loth, E., Baum, J., & Löhner, R. (1992). Vorticity produced by shock wave diffraction. Shock Waves, 2(1), 31-41.
[8] Chang, S. M., & Chang, K. S. (2000). On the shock-vortex interaction in Schardin's problem. Shock Waves, 10(5), 333-343.